



The determination of the focal spot size of an X-ray tube from the radiation beam profile



A.D. Oliveira^{a, b, *}, M.J. Fartaria^{a, 1}, J. Cardoso^a, L.M. Santos^a, C. Oliveira^{a, b}, M.F. Pereira^a, J.G. Alves^{a, b}

^a Universidade de Lisboa (UL), Instituto Superior Técnico (IST), Laboratório de Protecção e Segurança Radiológica (LPSR), Estrada Nacional 10 (ao km 139,7), 2986-066 Bobadela LRS, Portugal

^b UL-IST, Centro de Ciências e Tecnologias Nucleares (C2TN), Bobadela LRS, Portugal

HIGHLIGHTS

- A model of the X-ray beam profile allows the determination of the focal spot size.
- A general profile function fits the data measurements of the beam profile.
- Links between beam profile and line spread and edge spread functions are discussed.
- No need for additional or specific devices to estimate the focal spot size.

ARTICLE INFO

Article history:

Received 13 April 2015

Received in revised form

14 September 2015

Accepted 29 September 2015

Available online 3 October 2015

Keywords:

X-ray tube

Focal spot size

Beam profile

ABSTRACT

The aim of this work is to show that the focal spot size of a given X-ray tube can be determined from the profile of the radiation beam without the use of devices specifically designed for that task. The approach presented relies on a simple model for the radiation beam profile and on an analytical function used to fit the beam profile data. The basics of the profile function are outlined and the relationship between the fitting and the profile parameters are deduced. The relationship of the proposed method with the edge spread function and line spread function concepts is discussed. The focal spot size of an X-ray tube used at the Laboratory for Metrology of Ionizing Radiation (LMRI) of IST was determined using the proposed method. In the analysis of the experimental results, the heel-effect was also evaluated.

© 2015 Elsevier Ltd. All rights reserved.

1. Introduction

The focal spot of an X-ray tube is related with the beam profile and is a parameter of concern in both image and beam quality in diagnostic (Jain et al., 2014) and therapy (Baldwin and Fitchew, 2014). The X-ray beam profile at the detector plane can be characterized by the penumbra and the umbra generated by the combination of the focal spot and the collimation system (Baldwin and Fitchew, 2014) and the detector characteristics (Bub et al., 2007). Some of the characteristics of the detectors used in profile

measurements can influence the final result such as the detector size, the material and the electrical properties. The response of the detector can be modeled using the convolution theorem that connects the true profile and the measured profile by a convolution with the detector response function (Sibata et al., 1991; Kulmala and Tenhunen, 2012). The beam profile can be measured with detectors such as digital flat panels, for example, which have some resolution aspects to be considered (Bub et al., 2007). Film dosimetry has been found to be a straightforward and reliable method to obtain the beam profile (Sibata et al., 1991). Digital flat panels have replaced film technology; however, Gafchromic film was introduced which has a high spatial resolution. The accuracy and sensitivity of Gafchromic film depends highly on a proper film handling and development protocols and on a suitable and calibrated densitometry system (Kulmala and Tenhunen, 2012).

It is often assumed that the sigmoid shape of the penumbra is due to a Gaussian focal spot, leading to the use of an error function

* Corresponding author. Universidade de Lisboa (UL), Instituto Superior Técnico (IST), Laboratório de Protecção e Segurança Radiológica (LPSR), Estrada Nacional 10 (ao km 139,7), 2986-066 Bobadela LRS, Portugal.

E-mail address: adoliv@ctn.ist.utl.pt (A.D. Oliveira).

¹ Present address: Centre Hospitalier Universitaire Vaudois and University of Lausanne, Department of Radiology, CIBM, Lausanne, Switzerland.

for the simulation of the radiation beam profile (Dixon et al., 2005; Gambaccini et al., 2011; Salamon et al., 2008). However, other suitable sigmoid shaped functions, like the Fermi-Dirac function can be used without previous assumptions about the focal spot shape. In this work a Fermi-Dirac function was used as the basis of the beam profile model as suggested by Bistrovic (1978). An analytical function was used to fit the radiation intensity profile data of a given X-ray beam (Oliveira et al., 1995). The parameters of the profile function are directly related with the penumbras and umbra values. The profile function was used as a tool to determine the focal spot size adapting the well-known method of the edge spread function (Boone and Seibert, 1994; Gambaccini et al., 2011; Salamon et al., 2008).

Given a profile function and assuming a simple model for the radiation beam the necessary mathematical expressions to quantify the focal spot size can be derived.

At LMRI an X-ray tube was used to generate four different beams by varying the collimator openings. The profile data for each of the beams was experimentally obtained using an ionization chamber displaced along one of the axis on the detector plane.

Using the profile model the focal spot size was estimated and, furthermore, the heel-effect was also considered.

2. Materials and methods

2.1. The radiation beam set up

Due to technological reasons the actual focal spot size is different from the apparent focal spot size. The estimation of the apparent focal spot size, c , is the aim of this work. The electrons emitted from the filament are accelerated by the tube voltage striking the anode and defining the actual focal spot size. The inclination of the anode defines the apparent focal spot size, c , as illustrated in Fig. 1. In the model developed below the apparent focal spot is the projected focal spot in the anode–cathode direction which is independent of the anode inclination. The focal spot can be determined from the apparent focal spot multiplying by the sine of the anode inclination.

The radiation beam of a given X-ray tube defines a radiation profile at the image detector plane. Let us consider an X-ray tube with a given apparent focal spot (mentioned below as focal spot) that will generate a beam defined by a given collimator.

If the beam is oriented along the positive Z axis of a given referential, then the beam profile is defined in the XY plane (detector plane) as represented in Fig. 1. The beam profile can be described by a function along a given direction in the XY plane, for example along the X axis as a function $f(x)$.

The intensity distribution emitted from the focal spots falls between a rectangle and that of a two hot-spot sources or even more complex shapes (Wagner et al., 1974). In the simple model presented below, the focal spot are treated as a rectangle corresponding to a line segment in the 2D projection of Fig. 1.

The focal spot c and the collimation opening w of the beam are the cause of a certain level of penumbra in the radiation profile, at both sides of the edge of the beam, which can be named left (p_L) and right (p_R) penumbras. Due to the inclination of the anode the left and right penumbras are caused by different apparent focal spot sizes, c_L and c , respectively. Between the left and right penumbras an umbra, U , region is defined, corresponding to the main section of the beam, sometimes named “top flat zone” or “plateau”, where the dose or radiation intensity is ideally constant. The full width at half maximum (FWHM) can be defined as the distance between the middle points of both penumbras. A more rigorous definition of FWHM will be given below.

2.2. Focal spot size estimators

In this section three estimators for the focal spot size will be obtained. Let us consider that the collimator opening, w , is larger than the focal spot, c , by a value b_1 and b_2 , respectively on the left and right sides of the ZZ' axis (see Fig. 1) so that

$$b_1 + b_2 + c = w \quad (1)$$

At the XY image (or detector) plane the umbra value, U , depends on the magnification geometry. From Fig. 1, it follows that

$$a_1 + a_2 + c = U \quad (2)$$

From the equivalence of triangles we can write

$$b_2/F_c = a_2/F \quad (3)$$

Let us define a magnification factor, M , given by the ratio between F and F_c :

$$M = F/F_c \quad (4)$$

Where F and F_c are, respectively, the focal spot detector distance and the focal spot collimator distance. From Equations (3) and (4) follows

$$M = a_2/b_2 \quad (5)$$

Meaning that the value of a_2 is the magnification of b_2 or $a_2 = M b_2$. A similar equation is found for a_1 and b_1 . Then, the sum $a_1 + a_2$ is given by

$$a_1 + a_2 = M(b_1 + b_2) \quad (6)$$

Inserting Equation (6) in Equation (2) gives

$$M(b_1 + b_2) + c = U \quad (7)$$

From Equation (1) we have

$$(b_1 + b_2) = w - c \quad (8)$$

To finalize, from Equations (7) and (8) the focal spot size is given by

$$c = (Mw - U)/(M - 1) \quad (9)$$

The meaning of this equation is that if the magnification factor, M , the collimation opening, w , and the umbra, U , are known then it is possible to estimate the focal spot size, c .

Let us now consider both left and right penumbras shown in Fig. 1. Again by the equivalence of triangles we have

$$(c + b_2)/F_c = (c + a_2 + p_R)/F \quad (10)$$

Solving for c it turns out that:

$$c = p_R/(M - 1) \quad (11)$$

This is another expression for the focal spot size estimation obtained from the right penumbra, p_R , and the magnification factor, M . The same argument can be used for the left penumbra, p_L . Considering the anode inclination the apparent focal spot is now c_L instead of c (Fig. 1). Due to the equivalence of triangles

$$(c_L + b_1)/F_c = (c_L + a_1 + p_L)/F \quad (12)$$

As above, this leads to another expression for the focal spot size:

$$c_L = p_L/(M - 1) \quad (13)$$

Let us point out that from Equations (11) and (13) both the

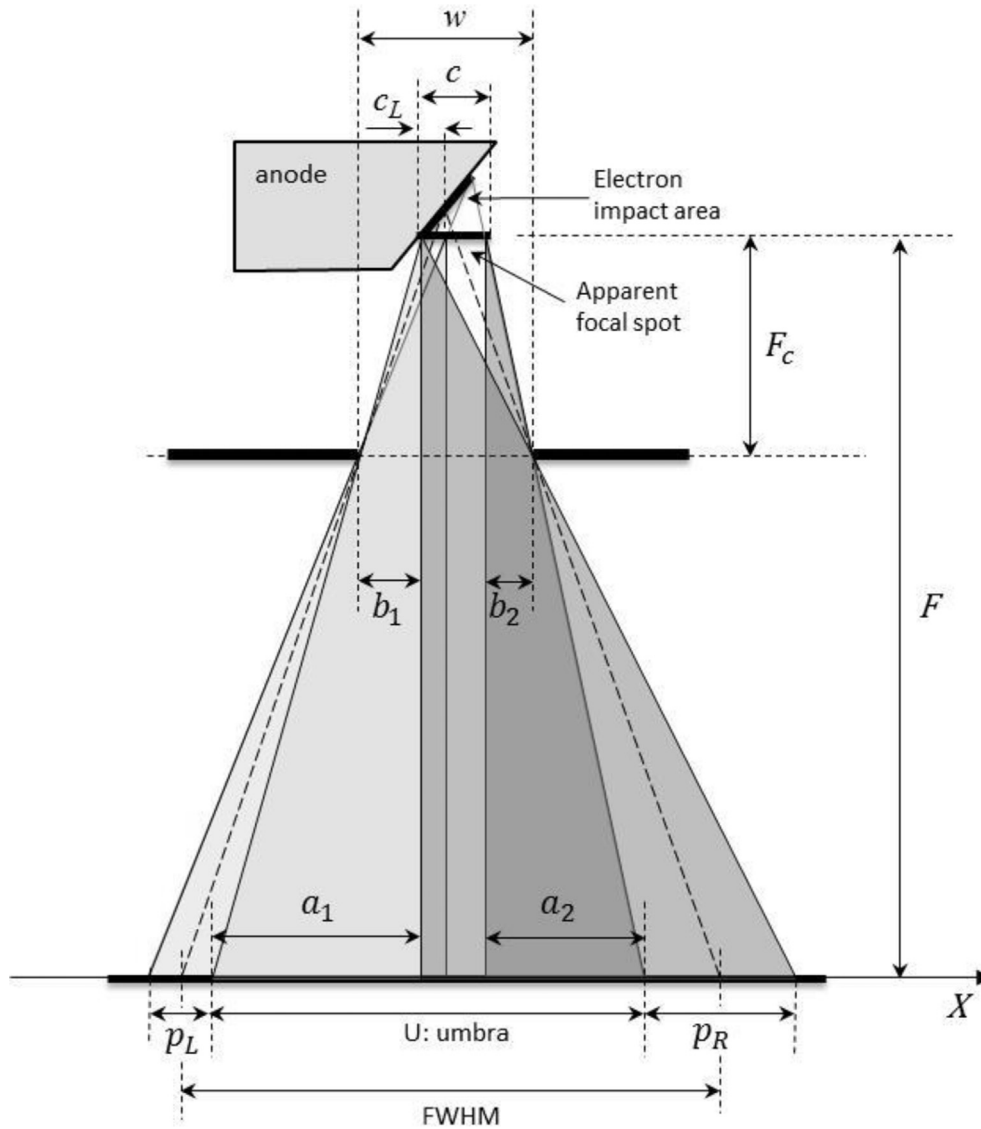


Fig. 1. Outline of an X-ray beam generated by an X-ray tube. The apparent focal spot size is represented by c or c_L , and the collimator has a w opening. The parameters of interest to characterize the beam profile are: left and right penumbra (respectively p_L and p_R), umbra (U) and full width at half maximum (FWHM).

penumbra and focal spot sizes are related. Gambaccini et al. (2011), used the slit method and found similar Equations to (11) and (13) for the focal spot size.

In conclusion, if both the left and right penumbras and the umbra, together with the magnification factor are known, three expressions, (9), (11) and (13) can be obtained that allow the quantification of the focal spot size. To distinguish the three estimators let us rename c as c_U and c_R , respectively for Equations (9) and (11), while c_L is given by Equation (13).

Making the profile measurements with several collimator openings allows extrapolation to zero. The final result of the focal spot value will be obtained by a zero extrapolation procedure obtained from the decreasing w values.

2.3. Beam profile function

In this section the beam profile function is defined and the parameters such as p_L , p_R , FWHM and U are determined. The profile function was developed as a sum of two sigmoid-shaped functions, inspired in the Fermi-Dirac distribution law each one with an

inflection point. Let us consider two sigmoid-shaped functions, named left (y_L) and right (y_R):

$$y_L(x) = [1 + \exp((1/n_L)(1 - (x/k)))]^{-1} \quad (14)$$

$$y_R(x) = [1 + \exp((1/n_R)((x/k) - 3))]^{-1} \quad (15)$$

The sum of both equations and its normalization to unity leads to:

$$f(x) = (1 + \exp(F + G)) / ((1 + \exp(F))(1 + \exp(G))) \quad (16)$$

where the functions $F=F(x)$ and $G = G(x)$ are given by

$$F(x) = (1/n_L)(1 - (x/k)) \quad (17)$$

$$G(x) = (1/n_R)((x/k) - 3) \quad (18)$$

Each Equations (14) and (15) has one inflection point; as a consequence, Equation (16) has two inflection points at the mid-points of the penumbras. To obtain the penumbras, a tangent line at

the inflection points of the profile curve was drawn to determine the abscissa value for the ordinates $y = 0$ and $y = 1$ of the tangent line. The distance between the orthogonal projections on the abscissa defines the penumbra. Using simple analytical geometry it can be shown that the penumbras are given by the expressions:

$$p_L = 1 / \left(\frac{df}{dx} \right)_{x=k} \quad (19)$$

$$p_R = -1 / \left(\frac{df}{dx} \right)_{x=3k} \quad (20)$$

From Equation (16), the Equations (19) and (20) give for p_L and p_R

$$p_L = 4kn_L / [1 - (2 / (1 + \exp(2/n_R)))] \approx 4kn_L \quad (21)$$

$$p_R = 4kn_R / [1 - (2 / (1 + \exp(2/n_L)))] \approx 4kn_R \quad (22)$$

Since both n_L and n_R are less than 0.1 then the denominators of Equations (21) and (22) are approximately 1, given:

$$p \begin{Bmatrix} L \\ R \end{Bmatrix} \approx 4kn \begin{Bmatrix} L \\ R \end{Bmatrix} \quad (23)$$

The FWHM is given by the difference between the abscissas of the inflection points of the right and left penumbras, $\text{FWHM} = 3k - k$, given

$$\text{FWHM} = 2k \quad (24)$$

As already mentioned above, the umbra, U , is the distance between both penumbras and it is easily show that is given by Equation (25).

$$U = \text{FWHM} - (p_L + p_R) / 2 \quad (25)$$

An additional parameter is introduced in the profile function in order to allow lateral shift L along the X axis, meaning that

$$f = f(x - L) \quad (26)$$

The shape of the function is independent of the lateral shift value. The fitting method determines the set of parameters, n_L , n_R , k and L that minimize the root mean square deviation (RMSD) between the experimental data and the fitting function. An EXCEL file with a Visual Basic® macro was developed that searches for the fitting parameters in a few minutes, however any other fitting software can be used.

In conclusion, in this section the Equation (16) provides a model to fitting the data from measurements of the beam profile, allowing us to determine important parameters such as the umbra, penumbras and FWHM.

2.4. Heel-effect

It is well-known that the umbra of a given beam profile, sometimes named “top flat” is often, in fact, not flat. This variation in the intensity is named heel-effect. The heel-effect results from a different intensity distribution over the focal spot area resulting in a umbra slightly tilted. The decrease in intensity along a line from the cathode to the anode, is principally due to the filtration of the Bremsstrahlung spectrum created within a thick target by overlying layers of target material (Fritz and Livingston, 1982). Without the heel-effect a perfectly top flatted profile would be expected. As mentioned above, for a given profile, the umbra is the distance between both, left and right, penumbras. From a mathematical

point of view, the umbra is the distance between two abscissa values, a left ($x_{U,L}$) and a right ($x_{U,R}$), given by the expressions $x_{U,L} = k + p_L/2$ and $x_{U,R} = x_{U,L} + U$, where k , U and p_L was already introduced above. In a first approximation, the heel-effect can be estimated by a linear fit of the profile data measured in the umbra zone. The slope of the linear fit can be used as a parameter to estimate and quantify the level of the heel-effect.

2.5. Edge spread function and line spread function

As stated above, the left and right penumbras are obtained by the inverse of the derivatives of the profile function at the inflection points $x = k$ and $x = 3k$, respectively (see Equations (19) and (20)). The aim of this section is to compare the method proposed with the well-known method of the edge spread function (ESF), often used to estimate the focal spot size (Gambaccini et al., 2011). The ESF is related with the line spread function (LSF) and the modulation transfer function (MTF) which are often used to assess the spatial resolution in radiology (Boone and Seibert, 1994; Gambaccini et al., 2011; Salamon et al., 2008).

It is well-known that the line spread function, LSF, is obtained by the derivative of the ESF (Salamon et al., 2008), that is:

$$\text{LSF}(x) = \frac{d}{dx} \text{ESF}(x) \quad (27)$$

Several analytical functions have been proposed to describe the ESF function (Gambaccini et al., 2011; Boone and Seibert, 1994). For comparison with the literature let us consider, for example, the ESF(x) Equation (8) of Gambacini et al. (2011) of the edge spread function, which is given by

$$\text{ESF}(x) = y_0 + A \operatorname{erf} \left((x - x_0) / \sigma\sqrt{2} \right) \quad (28)$$

Where y_0 and A are the parameters that determine the amplitude of the signal, x_0 is the center of the edge (mathematical inflection point) and sigma is the slope at the inflection point (Gambaccini et al., 2011). The LSF value at the inflection point, $x = x_0$ is given by Equation (27), which leads to:

$$\text{LSF}(x = x_0) = C \quad (29)$$

where C is a constant. At the ESF inflection point, the LSF has the maximum value.

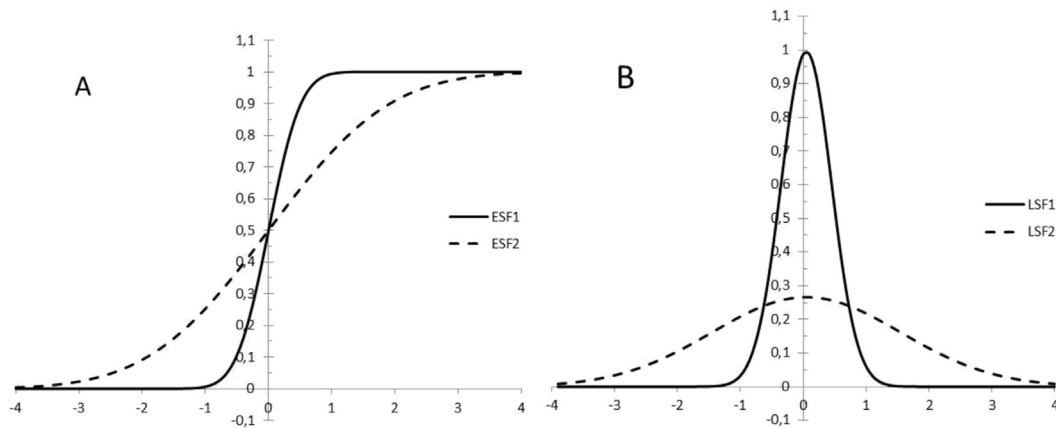
Let us point out that for the ESF inflection point, the inverse of the LSF(x) is exactly the Equation (19). Thus, for any sigmoid-shaped curve, a relationship between the profile function, the LSF and the penumbra was obtained, as follows:

$$p_L = 1 / \left(\frac{df}{dx} \right)_{x=k} = 1 / \text{LSF}(x = k) \quad (30)$$

An equivalent equation is valid for the right penumbra. The maximum of the LSF is given by the inverse of the penumbra value of a given ESF function, or in our case of a given radiation profile function.

This result shows a relationship between the spatial resolution and penumbra. In Fig. 2A two edge spread functions (ESF1 and ESF2) are shown, obtained from Equation (28), with two different sigma values, defining the slope at the inflection point. The correspondents line spread functions (LSF1 and LSF2) are shown in Fig. 2B.

From Equation (30) it follows that the penumbras of ESF1 and ESF2 of Fig. 2A are $p_1 = 1 / \text{LSF1}(0) = 1 / 0.99 = 1.01$ and $p_2 = 1 / \text{LSF2}(0) = 1 / 0.27 = 3.70$, respectively, in arbitrary units.



Figs. 2. A) Two examples of ESF(x) with $y_0 = A = 0.5$; $x_0 = 0$ and $\sigma = 0.4$ for ESF1 and $\sigma = 1.5$ for ESF2. B) The Line Spread Function LSF1 and LSF2 show maximum values at $LSF1(0) = 0.99$ and $LSF2(0) = 0.27$, respectively. Spatial dimension of the abscissa axis is arbitrary.

2.6. X-ray profile measurements

In order to minimize the broadening of the measured penumbras and avoiding volume averaging corrections a small ionization chamber was used to obtain the x-ray field profile. In effect, it was reported that for small enough ionization chambers the correction of the profile is small, being no more than 4%–5% on the steeply descending slope of the profile for chamber volumes of 0.1 cm^3 , with 3.5 mm sensitive diameter (Higgins et al., 1995). Thus, for small ionization chambers the uncorrected measurements are adequate for the profile measurement. A cylindrical ionizing chamber (PTW model 23332; rigid stem chamber 0.3 cm^3 , with 5 mm inner diameter) and associated electrometer (PTW UNIDOS) were used. Also, due to the very small variation response for radiation energy 50–150 keV (less than 3%) it was not considered any correction for energy response. The measurements (Oliveira, 2011) were carried out at LMRI using an X-ray tube Philips model MCN 165 (anode with 22° inclination).

The ionization chamber was positioned in such a way that the beam axis intersects the center of the chamber at the reference plane distance, in agreement with the calibration certificate. The characterization of the radiation field was performed in the radiation quality W/Mo for 28 kVp and 5 mA tube current. Four collimator openings were used to obtain four different radiation fields. The measurements were performed with the ionization chamber along one axis of the XY detector plane, at 2.5 mm intervals within the penumbra area and 5 mm or 10 mm in the top flat zones, along the horizontal axis defined at the center beam. Ten measurements (air kerma values) of 1 min each were obtained at each position. The measurements were corrected for the reference influence quantities, e.g. pressure, temperature and humidity and normalized in relation to the maximum value. The normalized air kerma measurements define the experimental radiation dose (or intensity) profile.

The collimation system defines the field dimensions. The uniformity and homogeneity of the field depend of the anode inclination (heel-effect), of the additional filtration used and the focus–reference plane distance. The geometry of the irradiation is shown in Table 1. The uncertainties of the collimator opening (w), the focal spot to detector distance (F) and focal spot to collimator distance (F_C) was 0.06 cm which by uncertainty propagation rules leads to uncertainty in the magnification factor (M) of 0.02 .

3. Results and discussion

In Fig. 3 the four beam profiles obtained with four different

collimator openings w (A: 2.80 cm, B: 1.82 cm, C: 1.72 cm and D: 1.52 cm) are shown. Error bars are within the symbols.

Fitting the profile function to the measurements data leads to the profile parameters listed in Table 2.

The average value of all the penumbra values from Table 2 (columns p_L and p_R) is 1.04 cm .

From the data in Table 2 and applying the Equation (30) in the left penumbra, p_L , and an equivalent equation to the right penumbra, p_R , the line spread function, LSF, at the left and right inflection points can be calculated. This LSF values corresponds to the maximum value of the LSF as outlined in Fig. 2. From Table 2 the average value of the left penumbra is $0.87 \pm 0.05 \text{ cm}$, which, using Equation (30) corresponds to a maximum LSF of $1.15 \pm 0.06 \text{ cm}^{-1}$. For the right penumbra the average value in Table 2 is $1.21 \pm 0.05 \text{ cm}$ corresponding to a maximum of LSF of $0.83 \pm 0.03 \text{ cm}^{-1}$. Additional analysis around the LSF and ESF concepts are outside the scope of this work.

In Table 3 the values of FWHM obtained from the fitting and obtained by the magnification of the collimator Mw are compared. Uncertainty of Mw and FWHM are 0.1 cm .

Applying Equations (9), (11) and (13) the focal spot size was calculated and the results are listed in Table 4. The ratio between the left and right penumbras was included in order to assess the profile asymmetry.

Accordingly to the X-ray tube manufacturer the nominal standard focus is 0.55 cm . However, in the manufacturer certificate of the X-ray tube the focal spot size estimated with a pinhole camera is $0.37 \text{ cm} \times 0.46 \text{ cm}$.

In Table 4, 12 values of the focal spot size ranging from 0.21 cm to 0.36 cm were obtained. The basic statistics (average and sample standard deviation) for the focal spot size obtained from measurements on the horizontal line crossing the central point of the beam was $0.27 \pm 0.05 \text{ cm}$, which is close to the dimensions in the manufacturer certificate.

For a good symmetry of the profile it is expected a ratio, p_L/p_R , near unity. However, from Table 4, this ratio ranges between 0.60 , for case A, to 0.86 , for case C. Given this asymmetry and by

Table 1

Geometric conditions of the radiation beams: w : collimator opening, F : focal spot to detector distance, F_C : focal spot to collimator distance, M : magnification factor.

Reference	w (cm)	F (cm)	F_C (cm)	$M = F/F_C$
A	2.80	52.8	11.3	4.67
B	1.82	52.8	11.3	4.67
C	1.72	52.8	11.3	4.67
D	1.52	52.8	11.3	4.67

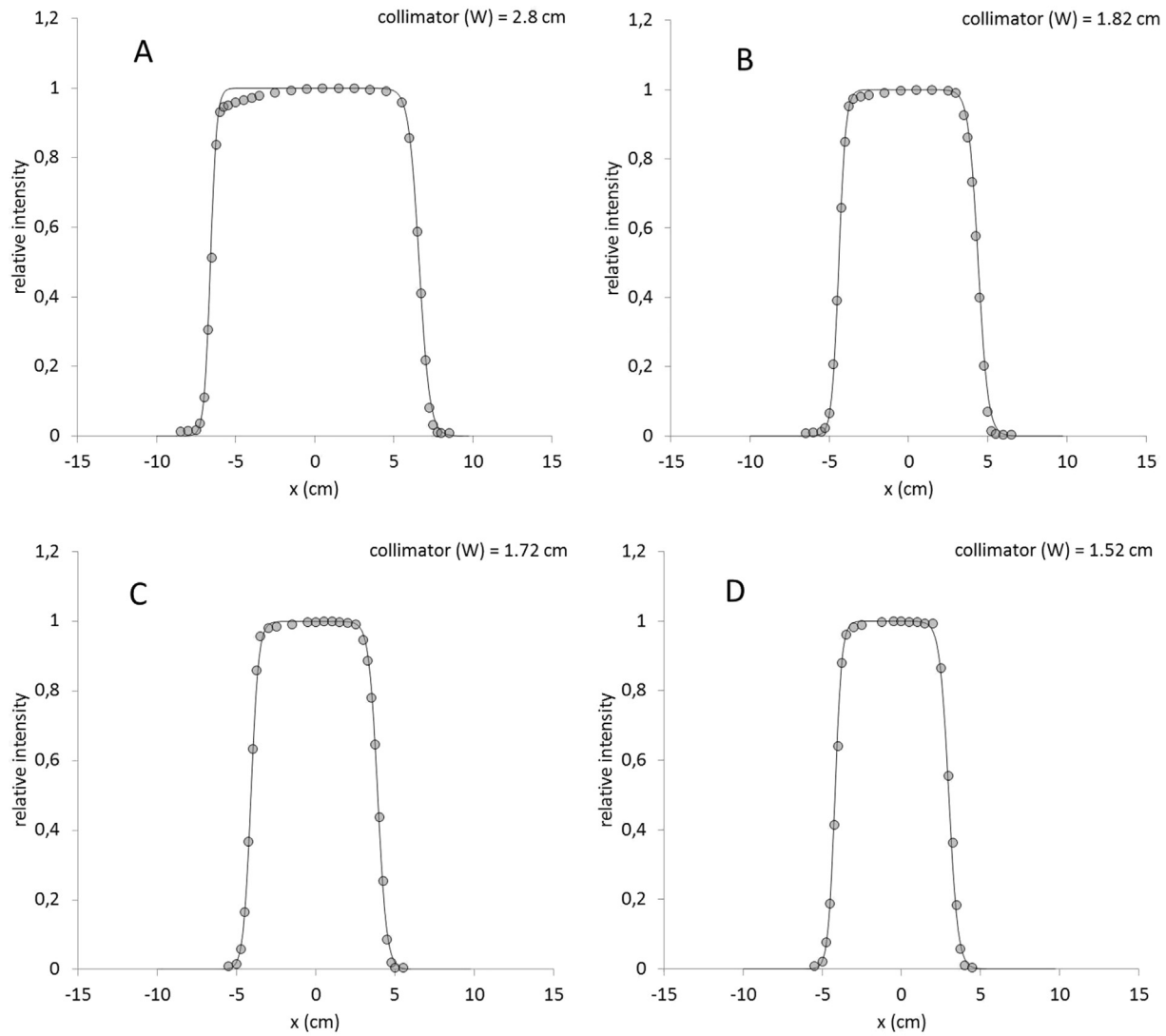


Fig. 3. Radiation beam profiles obtained with several collimator openings (*w*), A: 2.8 cm, B: 1.82 cm, C: 1.72 cm and D: 1.52 cm. The dots are normalized air kerma measurements performed with an ionization chamber at 2.5 mm intervals within the penumbra area and 5 mm or 10 mm in the top flat zones. The dark line represents the best fit to the experimental data. A magnification factor of $M = 4.67$ was considered. The uncertainty of the measurements was found to be 0.05% which is contained within the symbols (dots).

Table 2

Function and profile parameters relative to the measurement data from Fig. 3 (RMSD: root mean square deviation).

Ref.	Function fitting parameters					Profile parameters			
	n_L	n_R	k	L (cm)	RMSD	p_L (cm)	p_R (cm)	U (cm)	FWHM (cm)
A	0.03	0.05	6.6	-13.2	0.028	0.79 ± 0.13	1.32 ± 0.13	12.14 ± 0.14	13.2 ± 0.1
B	0.05	0.07	4.4	-8.8	0.022	0.88 ± 0.09	1.23 ± 0.09	7.74 ± 0.12	8.8 ± 0.1
C	0.06	0.07	4.0	-8.1	0.017	0.96 ± 0.08	1.12 ± 0.08	6.96 ± 0.12	8.0 ± 0.1
D	0.06	0.08	3.6	-7.8	0.023	0.86 ± 0.07	1.15 ± 0.07	6.19 ± 0.11	7.2 ± 0.1

Table 3

Comparison between the experimental data Mw and the FWHM determined from the profile function.

Ref.	M	w (cm)	Mw (cm)	FWHM (cm)	Relative deviation (%)
A	4.67	2.80	13.1	13.2	0.8
B	4.67	1.82	8.5	8.8	3.5
C	4.67	1.72	8.0	8.0	0
D	4.67	1.52	7.1	7.2	1.4

Table 4

Estimations of the focal spot size (c_U , c_L and c_R) and left and right penumbras ratio as a function of w .

Ref.	w (cm)	c_U (cm)	c_L (cm)	c_R (cm)	p_L/p_R
A	2.80	0.26 ± 0.05	0.22 ± 0.05	0.36 ± 0.05	0.60
B	1.82	0.21 ± 0.03	0.24 ± 0.02	0.33 ± 0.02	0.71
C	1.72	0.29 ± 0.04	0.26 ± 0.03	0.30 ± 0.03	0.86
D	1.52	0.25 ± 0.04	0.23 ± 0.03	0.31 ± 0.03	0.75

observation of the profiles in Fig. 4 it can be expected that the heel-effect has increasing importance by the following order: C, D, B and A. Considering that the umbra is defined between the abscissa values, $x_{U,L}$ and $x_{U,R}$ as mentioned above and considering the lateral shift parameter, L , the position of the umbra was determined. In Fig. 4 it is shown only the measurements in the umbra region. In order to evaluate the deviation of the umbra value from a top flat line a linear fitting was considered. The smaller the slope of the linear fitting the smaller the heel-effect is (Fig. 4).

Analyzing the slope of the linear fittings, the worst case was the collimation $W = 2.8$ cm (case A) showing the largest heel-effect (slope = 0.0047) while the more flat umbra was obtained by the collimation $W = 1.72$ cm (case C, slope = 0.0024) which have the smallest heel-effect. In conclusion, the heel-effect has increasing importance by the following order: C, B, D and A. Comparing with the results of the penumbra ratios, B and D cases are swapped, which leads to the conclusion that the ratio of the penumbras is not a suitable parameter to estimate the heel-effect. The slope of the linear fitting should be used instead.

To allow extrapolation of the focal spot size to point or zero collimation, four collimation opening values were used. The values of the focal spot size, from Table 4, as a function of the collimation opening (w) are shown in Fig. 5.

The linear regression of the data in Fig. 5 lead to the determination of the y-axis intercepts at 0.24 for c_U , 0.27 for c_L and 0.24 for c_R , with standard deviations for the intercepts of 0.08, 0.03 and 0.03 for c_U , c_L and c_R , respectively. The extrapolation to zero represents the focal spot size estimation for zero collimation opening. The average of the three extrapolation values and the corresponding uncertainty propagation lead to an estimation of the focal spot size of 0.25 ± 0.03 cm, which is slightly lower than the result of the basic statistics above (0.27 ± 0.05 cm).

Let us point out that the proposed method can be used with other detectors such as, for example, digital flat panels or Gafchromic film providing the appropriate corrections.

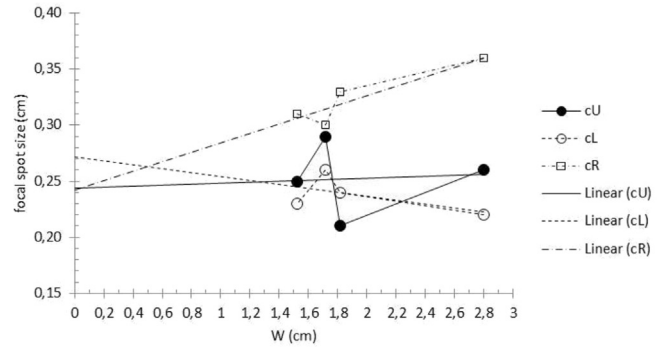


Fig. 5. Focal spot size as a function of the collimation opening (w). For better understanding of the graph, the error bars are not included. The uncertainty values are shown in Table 4.

4. Conclusion

Concerning the determination of the focal spot size of a given X-ray tube and unlike the known methods, the goal was accomplished without any device specifically designed to that purpose. A methodology was developed which is based in the analysis of experimental data from X-ray beam profiles. The radiation beam produced by an X-ray tube was characterized by a simple model with an umbra, penumbra and FWHM (full width half maximum), which is mainly due to the focal spot size of the equipment. For a given axis crossing a radiation beam perpendicular to the direction of incidence it can be defined a radiation profile along that axis. A mathematical model describing the profile of the X-ray beam was proposed. Three estimators of the focal spot size that depend on the magnification factor, the collimation opening, the umbra and the penumbras were obtained. Fitting the experimental profile with the proposed mathematical function, the umbra, penumbras and FWHM are obtained. In what concerns the heel-effect, the edge spread function and the line spread function, the relationships with

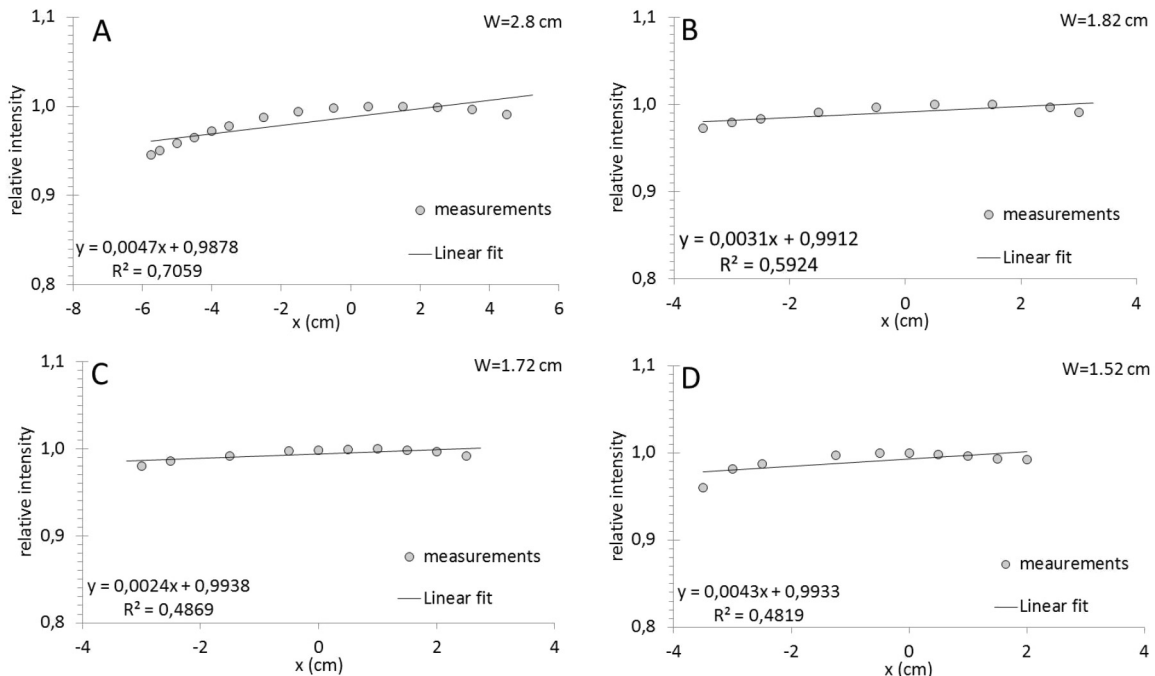


Fig. 4. Analysis of the heel-effect for collimator sizes: A: 2.8 cm, B: 1.82 cm, C: 1.72 cm and D: 1.52 cm.

the proposed approach were discussed.

One advantage of the proposed method is that it can be used with or without an image record device; for example, a dose monitor was used. As an example of application the focal spot of an X-ray tube used at the Laboratory for Metrology of Ionizing Radiation (LMRI) of IST was successfully determined using the proposed methodology and an ionization chamber.

References

- Baldwin, Z., Fitchew, R., 2014. The influence of focal spot size, shape, emission profile and position on field coverage in a Gulmay D3300 Kilovoltage X-ray therapy unit. *Australas. Phys. Eng. Sci. Med.* 37, 515–523.
- Bistrovic, M., 1978. A model for lateral profiles of ^{60}Co beams. *Phys. Med. Biol.* 23 (1), 171–172.
- Boone, J.M., Seibert, J.A., 1994. An analytical edge spread function model for computer fitting and subsequent calculation of the LSF and MTF. *Med. Phys.* 21 (10), 1541–1545.
- Bub, A., Gondrom, S., Maisl, M., Uhlmann, N., Arnold, W., 2007. Image blur in a flat panel detector due to Compton scattering at its internal mountings. *Meas. Sci. Technol.* 18, 1270–1277.
- Dixon, R.L., Munley, M.T., Bayram, E., 2005. An improved analytical model for CT dose simulation with a new look at the theory of CT dose. *Med. Phys.* 32 (12), 3712–3728.
- Fritz, S.L., Livingston, H., 1982. A comparison of computed and measured heel effect for various target angles. *Med. Phys.* 9 (2), 216–219.
- Gambaccini, M., Cardarelli, P., Taibi, A., Franconieri, A., Di Domenico, G., Marziani, M., Barnà, R.C., Auditore, L., Morgana, E., Loria, D., Trifirò, A., Trimarchi, M., 2011. Measurement of focal spot size in a 5.5 MeV linac. *Nucl. Instrum. Methods B* 269, 1157–1165.
- Higgins, P.D., Sibata, C.H., Siskind, L., Sohn, J.W., 1995. Deconvolution of detector size effect for small field measurement. *Med. Phys.* 22 (10), 1663–1666.
- Jain, A., Panse, A., Bednarek, D.R., Rudin, S., 2014. Focal spot measurements using a digital flat panel detector. *Proc. SPIE Int. Soc. Opt. Eng.* 9033 (0).
- Kulmala, A., Tenhunen, M., 2012. Super-resolution non-parametric deconvolution in modelling the radial response function of a parallel plate ionization chamber. *Phys. Med. Biol.* 57, 7075–7088.
- Oliveira, A.D., Alves, J.G., Carvalho, F., Carreiro, J.V., 1995. Dose profile and dose index analysis in computed tomography. *Radiat. Prot. Dosim.* 57 (1–4), 387–391.
- Oliveira, M.J., 2011. MSc Thesis, FCT, Universidade Nova de Lisboa.
- Salamon, M., Hanke, R., Kruger, P., Sukowski, F., Uhlmann, N., Voland, V., 2008. Comparison of different methods for determining the size of a focal spot of microfocus X-ray tubes. *Nucl. Instrum. Methods A* 59, 54–58.
- Sibata, C.H., Mota, H.C., Beddar, A.S., Higgins, P.D., Shin, K.H., 1991. Influence of detector size in photon beam profile measurements. *Phys. Med. Biol.* 36 (5), 621–631.
- Wagner, R.F., Weaver, K.E., Denny, E.W., Bostrom, R.G., 1974. Toward a unified view of radiological imaging systems. *Med. Phys.* 1 (1), 11–24.